



I_{Ks} ion-channel pore conductance can result from individual voltage sensor movements

Maartje Westhoff^a, Jodene Eldstrom^a, Christopher I. Murray^a, Emely Thompson^a, and David Fedida^{a,1}

^aDepartment of Anesthesiology, Pharmacology and Therapeutics, University of British Columbia, Vancouver, BC V6T 1Z3, Canada

Edited by Richard W. Aldrich, The University of Texas at Austin, Austin, TX, and approved March 6, 2019 (received for review July 5, 2018)

The I_{Ks} current has an established role in cardiac action potential repolarization, and provides a repolarization reserve at times of stress. The underlying channels are formed from tetramers of KCNQ1 along with one to four KCNE1 accessory subunits, but how these components together gate the I_{Ks} complex to open the pore is controversial. Currently, either a concerted movement involving all four subunits of the tetramer or allosteric regulation of open probability through voltage-dependent subunit activation is thought to precede opening. Here, by using the E160R mutation in KCNQ1 or the F57W mutation in KCNE1 to prevent or impede, respectively, voltage sensors from moving into activated conformations, we demonstrate that a concerted transition of all four subunits after voltage sensor activation is not required for the opening of I_{Ks} channels. Tracking voltage sensor movement, via [2-(trimethylammonium)ethyl]methanethiosulfonate bromide (MTSET) modification and fluorescence recordings, shows that E160R-containing voltage sensors do not translocate upon depolarization. E160R, when expressed in all four KCNQ1 subunits, is nonconducting, but if one, two, or three voltage sensors contain the E160R mutation, whole-cell and single-channel currents are still observed in both the presence and absence of KCNE1, and average conductance is reduced proportional to the number of E160R voltage sensors. The data suggest that KCNQ1 + KCNE1 channels gate like KCNQ1 alone. A model of independent voltage sensors directly coupled to open states can simulate experimental changes in I_{Ks} current kinetics, including the nonlinear depolarization of the conductance–voltage (G–V) relationship, and tail current acceleration as the number of nonactivatable E160R subunits is increased.

I_{Ks} | KCNE1 | KCNQ1 | voltage sensor | allosteric gating

KCNQ channels are a family of five voltage-gated potassium channels (VGKCs) found throughout the body, whose members all play important roles in health and disease (1). KCNQ1 (Q1) in the heart is required for regulation of cardiac action potential duration, and thus cardiac inotropy and dromotropy. Loss- and gain-of-function mutations have been implicated in long and short QT-interval syndromes, respectively (2–4), which can lead to serious ventricular arrhythmias and sudden death. Q1 channels are known to associate with KCNE1 (E1) subunits in the heart to form the I_{Ks} current and with other KCNE subtypes in many other tissues, although the full nature and diversity of their heteromultimeric interactions have still not been clearly elucidated (1).

The ratio of the number of Q1 to E1 subunits has been studied extensively, and while some report a fixed stoichiometry of four Q1 subunits for every two E1s (5–8), we and other groups have shown that a variable stoichiometry is possible, with anywhere between one and four E1s associating within the channel complex, depending on the concentration of E1 available (9–12). If channel complexes do exist with multiple E1:Q1 configurations, this would allow for greater flexibility upon modulation. This is because the presence of E1 subunits in the channel complex has a dramatic effect on all of the physiologically relevant properties of the channel, including “voltage-dependence, current kinetics, inactivation, single channel conductance, selectivity and pharmacology” (13). The profound changes that E1 can impose on Q1 channel properties have prompted a series of probing experimental and modeling studies over many years from a number

of different laboratories to understand the gating and pore functions of the Q1 channel, with and without E1.

Electrophysiological data have been used to define state models of Q1 (14) in the presence or absence of E1. These studies have been interpreted using the principles established by Hodgkin and Huxley (15) for potassium channels, where gating particles move independently, and once activated lead to pore opening via a concerted step, but do not affect ion permeation once the pore is open. This can be seen in the development of the models for Shaker channel gating, a member of the VGKC family (simplified in Fig. 1A) (16, 17). The voltage sensor (VS) domains undergo two independent transitions to reach an activated conformation, before all four subunits undergo one, or multiple, concerted transitions (17), at which point the pore is able to conduct current. The presence of a concerted transition between VS activation and pore opening is reflected experimentally in the degree of voltage displacement between direct gating current measurements of VS charge movement (Q–V) (18), or fluorescence measurements of VS movement (19–21), and the voltage dependence of the conductance–voltage (G–V) relationship (19). Similar observations of fluorescence–voltage (F–V) and G–V nonconcordance have been made in the I_{Ks} channel complex (22, 23), and led these authors to incorporate a concerted opening step in channel gating into their I_{Ks} models, with the implication that the VSs in all four subunits must be activated before pore opening can occur.

In contrast to this scheme of gating, others have suggested that the I_{Ks} channel pore may open before all VSs are activated. Using thermodynamic mutant cycle analysis with mutations that disrupt I_{Ks} channel opening, in either one, two, three, or all four S4 domains, Meisel et al. (24) noted that individual subunit

Significance

A potassium current in the heart (I_{Ks}) is important in regulating the heartbeat. These channels, composed of KCNQ1 and KCNE1 subunits, have four voltage-sensitive components and a pore component, which opens to allow current to pass through. The number of voltage-sensitive components required to activate to allow the pore to open has been debated extensively. While some believe all four are needed, others believe the pore can open with movement of a single voltage-sensitive component. Here, we show that the latter idea is correct, with movement of each component resulting in increasingly more current. This makes for a uniquely flexible channel, tunable for a broad range of responses.

Author contributions: M.W., J.E., C.I.M., and D.F. designed research; M.W., J.E., C.I.M., E.T., and D.F. performed research; M.W., J.E., E.T., and D.F. analyzed data; and M.W., J.E., and D.F. wrote the paper.

The authors declare no conflict of interest.

This article is a PNAS Direct Submission.

Published under the PNAS license.

¹To whom correspondence should be addressed. Email: david.fedida@ubc.ca.

This article contains supporting information online at www.pnas.org/lookup/suppl/doi:10.1073/pnas.1811623116/-DCSupplemental.

Published online March 27, 2019.

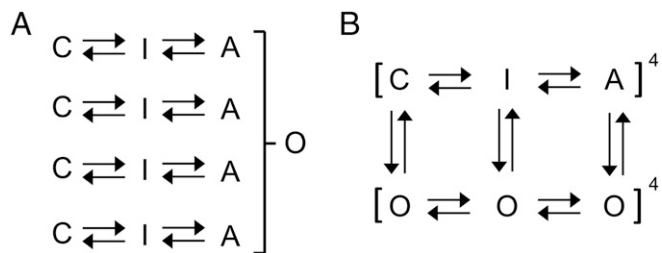


Fig. 1. Models of ion-channel gating. Simplified Markov schemes of I_{Ks} channel gating. (A) Independent gating domains each undergo two transitions, followed by a concerted step involving all four domains that leads to channel opening. Resting and intermediate states are represented by C and I, fully activated states are represented by A, and the open state is represented by O. (B) Allosteric model of channel gating in which pore opening may occur from all VS states. Resting, intermediate, and activated closed states are represented by C, I, and A, respectively. Open states are represented by O. Voltage-dependent transition rates of the VS are denoted by horizontal arrows. Transition rates between open and closed states are denoted by vertical arrows. Fourth-power notation represents the four VSs.

movement contributed sequentially to channel conductance, rather than a concerted step being required. They likened I_{Ks} gating to the allosteric model of gating proposed for Q1 alone (22), where the pore can open or close regardless of the position of the VSs, even when they are at rest (25). As more VSs are activated, the pore has a higher open probability, exemplified by voltage activation of the BK channel, a voltage- and calcium-activated potassium channel (26). The physical association of E1 (or PIP₂) significantly influences but does not materially change the underlying allosteric gating mechanism of Q1 (13, 27) but regulates the coupling rates between the various closed and open states. In Fig. 1B, a simplified version of this allosteric model of gating is shown, where VSs undergo two transitions to full activation, and in the presence or absence of KCNE1 each VS state is more or less coupled to corresponding open states of the channel (13, 27). Recent support for an allosteric I_{Ks} gating pathway comes from the modeling studies of Ramasubramanian and Rudy (28) in which pore openings to small or intermediate subconductance levels are shown to be possible over a range of early and intermediate S4 translations.

In this study, we have experimentally addressed the question discussed above, whether the I_{Ks} channel complex can open and conduct current before all four VSs have moved. We utilized the E160R and F57W mutations (13, 29, 30) in Q1 and E1, respectively, in tandem or quadruple constructs, to restrain between one and four VSs in their resting conformations, and studied them using whole-cell and single-channel patch-clamp techniques. Our results suggest that activation of all four VSs is not required for the I_{Ks} channel to conduct current, and thus that in I_{Ks} channels a final concerted transition is not obligatory for the pore to open but rather channels are better represented by a model where the pore can open from multiple closed-channel conformations, once one or more VS domains have entered an activated conformation.

Results

Channels with the E160R Mutation in All Four Q1 Subunits Are Nonfunctional. In wild-type (WT) channels, the VS domains of Q1 respond to changes in the membrane potential in a manner that eventually increases channel pore open probability. Interactions between the negative charge, E160, in the S2 domain with the positive charges in the S4 domain facilitate the movement of the VS (Fig. 2A, *Left*) (13). Movement of the VS, via its coupling to the pore, allows the pore to open and conduct current (31). By converting the negatively charged glutamic acid in the S2 of Q1 into a positively charged arginine, E160R, it is proposed that,

via electrostatic repulsion, the VS is prevented from moving into intermediate or activated conformations (13) (Fig. 2A, *Right*).

To investigate channel function when all four VSs are prevented from reaching an activated conformation, a 1:1 construct where the C terminus of E1 was tethered to the N terminus of Q1 (KCNE1-KCNE1; EQ) was used. To determine the $V_{1/2}$ of activation, a 4-s activation protocol ranging from -80 to $+100$ mV, or higher, was used (Fig. 2B). WT EQ (31.5 mV) produces currents with a similar $V_{1/2}$ of activation to WT Q1 + E1 [26.1 mV; (10)] (Fig. 2C and *SI Appendix*, Table S1). E160R EQ* (EQ*) channels have the E160R mutation in all four Q1 subunits, and do not produce a recognizable signal over the endogenous current of untransfected tsA201 cells (Fig. 2D and E), as well as having a similar current density (Fig. 2F). This phenomenon was previously described for E160R Q1* \pm E1 expressed in oocytes, by others (13, 29). Additionally, it has previously been shown that this lack of current is not due to a trafficking problem, as a biotinylation assay in oocytes indicated that the mutant channels are able to reach the membrane (32), though we cannot rule out that trafficking may be different in the mammalian cells we utilize for our experiments.

I_{Ks} Channels with One, Two, or Three VSs Containing the E160R Mutation Are Functional.

To investigate what happens to channels when one, two, or three VSs express the E160R mutation, constructs with tethered Q1 and/or E1 subunits were used [(E)QQ or (E)QQQQ]. The E160R mutation was incorporated into Q1 subunits of each construct to produce a channel complex where either one (E160R Q*QQQ; hereafter referred to as Q*QQQ), two (E160R Q*Q; hereafter referred to as Q*Q), or three (E160R EQ*QQ*Q*; hereafter referred to as EQ*QQ*Q*) VSs are suggested to be held down. In all of these situations, robust I_{Ks} -like currents were observed (Fig. 3), with at first glance only minor differences between the mutant and WT currents.

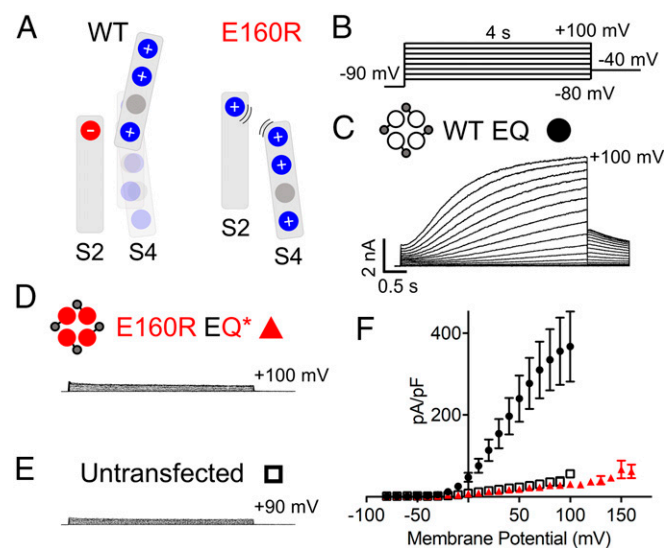


Fig. 2. E160R EQ* is a nonfunctional channel. (A) Cartoons representing the putative interactions between charges within the S2 and S4 domains of Q1 during normal activation in WT channels (*Left*) and when S4 movement is impeded by the presence of E160R (*Right*). (B) Currents were obtained using an isochronal 4-s activation protocol with pulses from -80 to $+100$ mV, or higher. Sweep-to-sweep intervals were 15 s. (C–E) Representative currents are shown for WT EQ (C), E160R EQ* (D), and untransfected cells (E). Cartoons describe the mutations in the constructs: E1 (small gray circles), WT Q1 (unfilled circles), and E160R Q1 (red circles). Black lines indicate tethers between subunits. (F) Plot representing the peak current density of WT EQ (black circles; $n = 3$), E160R EQ* (red triangles; $n = 42$), and untransfected cells (black open squares; $n = 4$) at various membrane potentials. Error bars denote mean \pm SE.

When expressed in the absence of E1, WT QQQQ and WT QQ (*SI Appendix, Figs. S1A and S2A*) produced currents with a similar $V_{1/2}$ to that previously reported for Q1 alone (-21.9 and -19.6 mV; *SI Appendix, Fig. S1E and Table S1*) (10). When one VS contains E160R (Q*QQQ), there was no significant shift in the $V_{1/2}$ of activation compared with WT, with a $V_{1/2}$ of -18.0 mV, but when two VSs contain the E160R mutation (Q*Q), the mean $V_{1/2}$ of activation was significantly depolarized by 17 to -3.0 mV. Also, the slope of the G–V relationship was reduced from 14.5 to 18.6 mV (*SI Appendix, Fig. S1 B–E and Table S1*).

Expression of WT constructs with E1-GFP (hereafter referred to as E1), WT QQQQ + E1 (Fig. 3A) and WT QQ + E1 (*SI Appendix, Fig. S2B*) produced normal-looking I_{Ks} currents with similar $V_{1/2}$ s to that previously reported for fully saturated I_{Ks} (32.1 and 34.1 mV; *SI Appendix, Table S1*) (10). Interestingly, Q*QQQ + E1 (Fig. 3B) currents have a similar $V_{1/2}$ to WT (33.6 mV; Fig. 3E and F and *SI Appendix, Table S1*). With Q*Q + E1 (Fig. 3C), the channel pore was still able to conduct current; however, as for constructs without E1, the mean $V_{1/2}$ of activation was significantly depolarized by 16 to 49.9 mV (Fig. 3E and

F and *SI Appendix, Table S1*). Next, the location of the two E160R mutations within the tandem construct was altered from opposing (Q*Q) to adjacent Q1 subunits (E160R QQQ*Q*; QQQ*Q*). QQQ*Q* + E1 had a similar depolarized $V_{1/2}$ of activation (55.6 mV) as Q*Q + E1 (49.9 mV) (P value = 0.31), indicating that there was no significant difference in the $V_{1/2}$ of activation when changing the location of the two E160R subunits (*SI Appendix, Fig. S3 A–C and Table S1*). Of note, when two E160R subunits were present in the channel complex, the mean whole-cell current density was reduced by about 60%, from 392.3 pA/pF to 142.4 at +60 mV (*SI Appendix, Fig. S4*).

When three VSs contain E160R (EQ*QQ*Q* + E1) (Fig. 3D), the currents produced had a very low macroscopic conductance and a further depolarized $V_{1/2}$ of activation (62.1 mV; Fig. 3E and F and *SI Appendix, Table S1*), along with a shallower slope (22.7 mV). In addition, the mean whole-cell current density with three E160R mutations was further reduced to 64.3 pA/pF at +60 mV (*SI Appendix, Fig. S4*). There is a clear nonlinear relationship between the $V_{1/2}$ s of activation for WT I_{Ks} currents and those containing one, two, or three E160R mutant subunits, along with an acceleration of tail current deactivation. What is noticeable, though, is that although the $V_{1/2}$ is displaced to more positive potentials with more E160R subunits, the values at the foot of the G–V relations are not significantly different (Fig. 3E, *Inset*).

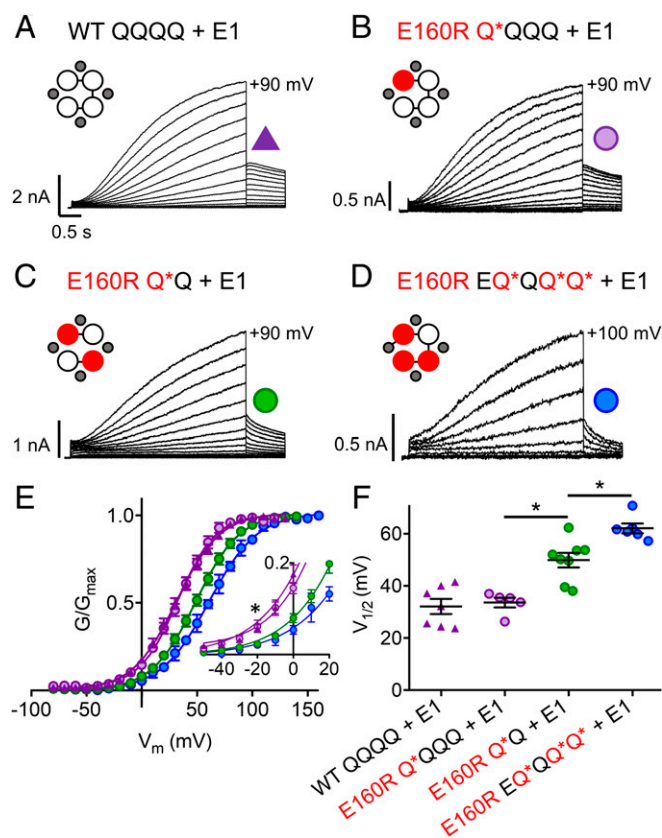


Fig. 3. I_{Ks} channel complexes with one, two, or three E160R mutations produce currents. Currents were obtained using the same isochronal activation protocol shown in Fig. 2B (E160R EQ*QQ*Q* + E1 data were recorded in 10- or 20-mV steps). (A–D) Representative currents are shown to +90 mV for WT QQQQ + E1 (A), E160R Q*QQQ + E1 (B), E160R Q*Q + E1 (C), and +100 mV for E160R EQ*QQ*Q* + E1 (D). Cartoons describe the mutations in the constructs: E1 (small gray circles), WT Q1 (unfilled circles), and E160R Q1 (red circles). Black lines indicate tethers between subunits. (E) G–V plots of WT QQQQ + E1 (purple triangles), E160R Q*QQQ + E1 (purple circles), E160R Q*Q + E1 (green circles), and E160R EQ*QQ*Q* + E1 (blue circles). (E, *Inset*) Expanded view of the curve between -50 and $+20$ mV ($*P < 0.05$ for ANOVA done on values between -50 and -20 mV). (F) Summary of the $V_{1/2}$ of activation for each construct ($n = 5$ to 8 ; $*P < 0.05$; *SI Appendix, Table S1*). Error bars denote mean \pm SE.

Subunits with the E160R Mutation Are Not Excluded from Channel Assembly.

To confirm that the relatively mild changes in the channel kinetics with additional E160R mutations were not due to the exclusion of E160R subunits from the channel complex, the tetraethylammonium chloride (TEA⁺) sensitivity of channels was examined (*SI Appendix, Fig. S5*). Previously, others have shown that WT Q1 + E1 channels are insensitive to addition of up to 50 mM TEA⁺ extracellularly (33), and introduction of the V319Y mutation into the outer pore of Q1 increases the channel's sensitivity to TEA⁺ (33). Here, we too show that addition of 2 and 50 mM TEA⁺ to WT EQQ + E1 channels (*SI Appendix, Fig. S5 A and D*; $n = 4$; P value between control and 50 mM = 0.9209) does not significantly reduce the peak current. Inclusion of V319Y in the first Q of EQQ (V319Y EQQ) increased the sensitivity to TEA⁺, with 2 mM TEA⁺ causing an $\sim 25\%$ reduction in peak current ($n = 6$; $P < 0.0001$), an effect which was reversed upon wash-off. E160R/V319Y EQ*Q has the E160R and V319Y mutations in the same subunit, and produces currents with a very low conductance. Addition of 2 mM TEA⁺ to E160R/V319Y EQ*Q + E1 had a similar effect to that on the V319Y mutant alone, with a reduction in peak current of $\sim 27\%$ ($n = 4$; $P < 0.0001$), which was reversed upon wash-off with control solution (*SI Appendix, Fig. S5 C and D*). Dose–response relationships for V319Y EQQ and E160R/V319Y EQ*Q overlay one another, with IC₅₀s for external TEA⁺ of 5.3 mM for both (*SI Appendix, Fig. S5D*). This result indicates that subunits containing the E160R mutation are not excluded from I_{Ks} channel complexes during assembly, and shows an identical TEA⁺ responsiveness, which suggests a uniform population of expressed channels.

Activation Kinetics of I_{Ks} When One, Two, or Three VSs Express the E160R Mutation.

To investigate whether inclusion of E160R in one, two, or three VSs alters the activation kinetics of the I_{Ks} channel, current waveforms between +50 and +160 mV were fit with a single exponential starting at 0.5 s (*SI Appendix, Fig. S6 A–F*) and activation time constants (τ_{act} s) extracted and plotted against the membrane potential. Noting that this method of fitting omits most of the delay during channel activation, there was no difference between the τ_{act} –V curve for WT QQQQ + E1, WT QQ + E1, and WT EQQQQ + E1 (*SI Appendix, Fig. S6G*). For channels where one VS contains E160R (Q*QQQ + E1), the τ_{act} –V curve overlays that of WT QQQQ + E1 (Fig. 4A),

whereas when two VSs contain E160R ($Q^*Q + E1$), the τ_{act-V} curve was depolarized compared with the WT, consistent with the ~ 16 -mV depolarizing shift in the $V_{1/2}$ of activation. For three VSs with E160R ($EQ^*QQ^*Q^* + E1$), the τ_{act-V} curve overlaps with that of two VSs containing E160R. If this curve were to be corrected for the ~ 30 -mV depolarization in $V_{1/2}$ from the WT, it would be hyperpolarized to the WT τ_{act-V} curve, which suggests an acceleration of current activation kinetics in $EQ^*QQ^*Q^* + E1$ (Fig. 4A).

Rate of Deactivation Increases Progressively as Multiple VSs Are Held Down. To investigate changes in the deactivation rate, the protocol shown in *SI Appendix, Fig. S7A* was used. The resulting tail currents were fit with a single exponential curve from which a deactivation time constant (τ_{deact}) was extracted (*SI Appendix, Fig. S7 B–G*) and plotted against the membrane potential. WT $QQQQ + E1$, WT $QQ + E1$, and WT $EQQQQ + E1$ had very similar τ_{deact} s at different membrane potentials, and significance tests indicated no difference between the deactivation rates when two or four Q1s are linked together (*SI Appendix, Fig. S7H*). $Q^*QQQ + E1$ channels deactivated faster than WT (Fig. 4B and *SI Appendix, Fig. S7E*), significantly so at -50 and -60 mV. With $Q^*Q + E1$, the rate of deactivation was further increased (Fig. 4B and *SI Appendix, Fig. S7F*), and was significantly different from WT at -50 , -60 , and -90 mV. Deactivation rates for $EQ^*QQ^*Q^* + E1$ were even faster, significantly so at -50 to -100 mV (not -70 or -80 mV) (Fig. 4B and *SI Appendix, Fig. S7G*). These data indicate that as more VSs contain E160R, there is a progressive increase in the rate of deactivation.

Single-Channel Recordings Show Reduced Conductance of Channels with E160R Subunits. To further understand the effects of preventing one, two, or three VSs from reaching activated conformations on I_{Ks} currents at the microscopic level, single-channel recording was used. Constructs with and without tethered E1s [(E) $Q^*QQQ + E1$, (E) $Q^*Q + E1$, and $EQ^*QQ^*Q^* + E1$] were utilized. At the whole-cell level, the tethered E1 does not interfere with the activation kinetics of I_{Ks} (*SI Appendix, Fig. S8 and Table S1*). Previously, we have reported the single-channel characteristics of the I_{Ks} channel (10, 34) and, in Fig. 5B, we again show that when cells are pulsed to $+60$ mV for 4 s, WT EQ channels open through multiple sublevels, with the histogram of opening

event amplitudes of the representative sweep and average of 49 sweeps (Fig. 5F and G, black) showing a dominant peak at 0.42 pA. Channel complexes where one VS contains E160R, $EQ^*QQQ + E1$, produced currents with a flickering phenotype (Fig. 5C). While most events were to smaller conductance levels, the channel can infrequently open to the main level seen in the WT EQ channel (Fig. 5F, purple). The all-points histogram of 49 sweeps of $EQ^*QQQ + E1$ shows a similar trend, with a reduced number of events at larger amplitudes and an increase in those at lower conductance levels (Fig. 5G, purple).

When two VSs contain the E160R mutation, conductance was further reduced (Fig. 5D), with the majority of the events occurring at ~ 0.2 pA and smaller (Fig. 5F, green), better highlighted by the all-points histogram of multiple sweeps shown in Fig. 5G. A similar result is seen when two E160R mutations are located in adjacent subunits ($QQQ^*Q^* + E1$) (*SI Appendix, Fig. S3 D and E*), correlating with the whole-cell data (*SI Appendix, Fig. S3 A–C*). Interestingly, although the channels with two E160R mutations reach lower amplitudes most of the time, they are occasionally still able to reach higher conductance levels, with events occurring at ~ 0.4 pA (Fig. 5F and G, green).

In channel complexes with E160R in three VSs, there was a continuing trend toward brief, flickering bursts of opening to lower conductance levels (Fig. 5E). The histogram of the representative sweep (Fig. 5F, blue) shows openings to a main peak of 0.08 pA, as does the all-points histogram of 49 sweeps of $E160R EQ^*QQ^*Q^* + E1$ (Fig. 5G, blue).

Ensemble average single-channel currents from channel complexes containing different numbers of E160R subunits are shown in Fig. 6. Fig. 6, *Left* shows individual patch currents from at least three cells in each construct, and Fig. 6, *Center* shows the averages of concatenated files from these cells. The averages demonstrate the decreased mean conductance with increasing numbers of E160R subunits, which is also seen in whole-cell data (Fig. 6, *Right* and *SI Appendix, Fig. S4*). There is also a decreasing latency, clearly seen in the ensemble average and whole-cell $E160R EQ^*Q + E1$ data, compared with the WT. Overall, the data demonstrate that the latencies and waveforms of averaged single-channel activity are closely consistent with whole-cell currents.

F57W, a Depolarizing E1 Mutant, Corroborates the E160R Data. Whole-cell recordings from I_{Ks} complexes containing different numbers of the E1 mutant F57W, which is known to drastically depolarize the $V_{1/2}$ of I_{Ks} (30), provide supportive data (*SI Appendix, Fig. S9*) to our results with E160R. Replacement of phenylalanine with the bulkier tryptophan in F57W is likely causing steric hindrance that must be overcome to drive the channel complex from the closed to open state (30).

One E1 mutated with F57W ($F57W E'QQQQ + E1$) had a similar $V_{1/2}$ to the WT (34.8 mV; *SI Appendix, Fig. S9 C and D and Table S1*), whereas the $V_{1/2}$ of two mutated E1s ($F57W E'QQ + E1$) was depolarized by ~ 10 mV (to 42.3 mV), and there was an acceleration of the deactivation rate (*SI Appendix, Fig. S9B*). Unlike EQ^* , four F57W E1s in the complex ($F57W E'Q$) still allowed the channel to conduct, but with a $V_{1/2}$ of 106 mV, and a much shallower G–V relationship (*SI Appendix, Fig. S9B and Table S1*). Additionally, there was an acceleration of the deactivation rate (*SI Appendix, Fig. S9B*). At the single-channel level, there were subtle differences between complexes containing the E160R mutation and those containing the F57W mutation. Like the E160R-containing mutants, the F57W mutants showed a reduction in the overall conductance levels, with increasing numbers of mutated subunits. *SI Appendix, Fig. S9E* shows examples of active single-channel sweeps of $Q^*Q + E1$ and $F57W E'QQ + E1$. While both channel types largely occupy lower conductance levels, it is clear that F57W-containing channels showed brief visits to higher conductance levels (*SI Appendix, Fig. S9F*).

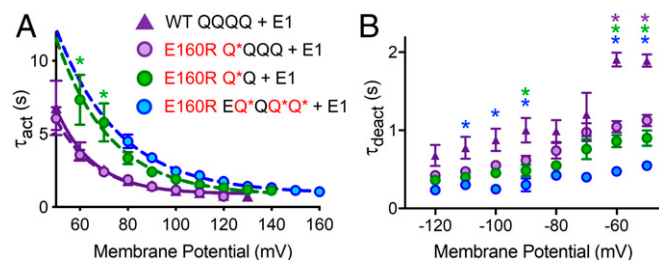


Fig. 4. Activation and deactivation kinetics of complexes with one, two, or three E160R mutations. The time constants of I_{Ks} current activation (τ_{act}) (A) and deactivation (τ_{deact}) (B) at various membrane potentials were plotted for WT $QQQQ + E1$ (purple triangles), E160R $Q^*QQQ + E1$ (purple circles), E160R $Q^*Q + E1$ (green circles), and E160R $EQ^*QQ^*Q^* + E1$ (blue circles) ($n = 5$ to 10). τ_{act} vs. membrane potential was fit with a single exponential equation to produce a τ_{act-V} curve for WT $QQQQ + E1$ (purple line), E160R $Q^*QQQ + E1$ (dashed purple line), E160R $Q^*Q + E1$ (dashed green line), and E160R $EQ^*QQ^*Q^* + E1$ (dashed blue line). * $P < 0.05$ on ANOVAs done between WT $QQQQ + E1$ and either E160R $Q^*QQQ + E1$ (purple asterisks), E160R $Q^*Q + E1$ (green asterisks), or E160R $EQ^*QQ^*Q^* + E1$ (blue asterisks). N.B. Fits were difficult to obtain at -70 and -80 mV due to small currents around the K^+ equilibrium potential, and this may explain the lack of significant differences at these potentials. Error bars denote mean \pm SE.

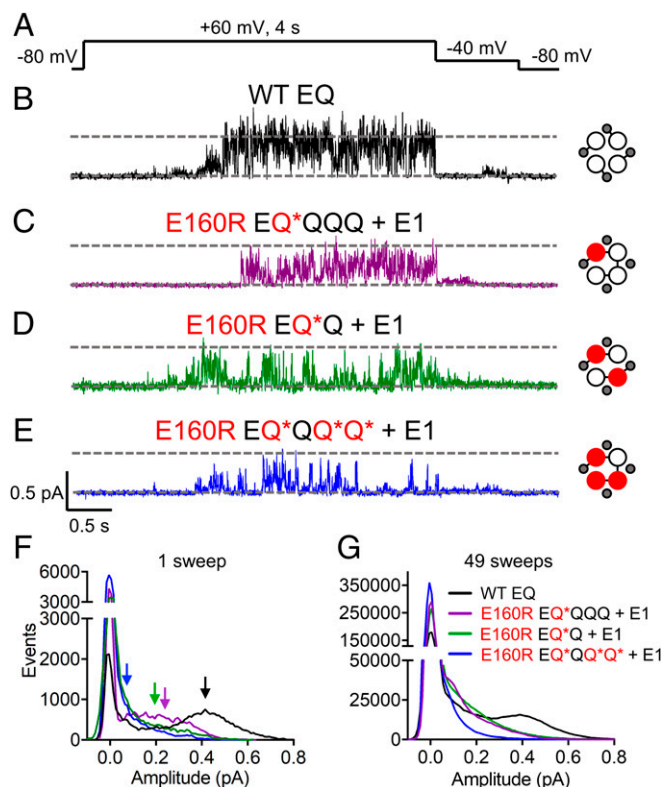


Fig. 5. Single-channel recordings of I_{Ks} complexes with one, two, or three E160R mutations. (A) Single-channel currents were obtained using a protocol where cells were stepped from -80 to $+60$ mV for 4 s, followed by a tail current at -40 mV. Sweep-to-sweep intervals for single-channel recordings were 10 s. (B–E) Representative single-channel traces are shown for WT EQ (B), E160R EQ*QQQ + E1 (C), E160R EQ*Q + E1 (D), and E160R EQ*QQ*Q* + E1 (E). Cartoons describe the mutations in the constructs: E1 (small gray circles), WT Q1 (unfilled circles), and E160R Q1 (red circles). Black lines indicate tethers between subunits. (F) All-points histograms for the displayed single sweep of WT EQ (black), E160R EQ*QQQ + E1 (purple), E160R EQ*Q + E1 (green), and E160R EQ*QQ*Q* + E1 (blue) are shown. Arrows highlight the amplitude peak in the open event distribution of each histogram based on Gaussian fits in Clampfit (0.42 pA for WT EQ, 0.25 pA for E160R EQ*QQQ + E1, 0.2 pA for E160R EQ*Q + E1, and 0.08 pA for E160R EQ*QQ*Q* + E1). (G) All-points histograms for 49 active sweeps combined from multiple cells of WT EQ [black line; $n = 5$ (cell 1: 6 sweeps; cell 2: 8 sweeps; cell 3: 12 sweeps; cell 4: 10 sweeps; cell 5: 13 sweeps)], E160R EQ*QQQ + E1 [purple line; $n = 3$ (cell 1: 35 sweeps; cell 2: 3 sweeps; cell 3: 11 sweeps)], E160R EQ*Q + E1 [green line; $n = 3$ (cell 1: 22 sweeps; cell 2: 18 sweeps; cell 3: 9 sweeps)], and E160R EQ*QQ*Q* + E1 [blue line; $n = 3$ (cell 1: 22 sweeps; cell 2: 20 sweeps; cell 3: 7 sweeps)].

Vs with the E160R Mutation Cannot Reach Intermediate or Activated States. To ensure that the E160R mutation prevents the VS from reaching an intermediate or activated conformation, extracellular [2-(trimethylammonium)ethyl]methanethiosulfonate bromide (MTSET) modification was used to track the external displacement of the VSs during channel activation in mammalian cells. To investigate this, two constructs were created. For both, a QQ fusion construct with a cysteine-less background (C214A/C331A) in both Q1 subunits was used. In the first construct, the MTSET G229C probe was in the first Q1, and the second Q1 contained the E160R mutation (G229C Q-Q*). The second construct had both the E160R and G229C mutations in the first Q1 (G229C Q*Q-Q). When both MTSET fusion constructs were expressed in the presence of E1, they produced currents with a similar $V_{1/2}$ of activation, 40 to 42 mV (SI Appendix, Fig. S10 A–D and Table S1). However, the G229C Q-Q* + E1 currents clearly had a faster rate of activation and produced currents that were less sigmoidal. This is likely

due to the effect of the G229C mutation to delay deactivation, as increasing the sweep-to-sweep interval to 60 s resulted in a more sigmoidal activation (SI Appendix, Fig. S10 E–G).

It is known that MTSET modification of G229C Q1 + E1 results in currents that do not fully deactivate at -90 mV, and thus show a loss of sigmoidicity during activation and a constitutive current (35). In Fig. 7, cells were pulsed to $+60$ mV for 4 s. After reaching a stable baseline, 2 mM MTSET was added to the bath at sweep 6. For G229C Q-Q* + E1, the instantaneous current dramatically increased, while the shape also became less sigmoidal (Fig. 7A). A diary plot of MTSET modification shows that, after addition of 2 mM MTSET, the time to half-maximum activation ($t_{1/2}$) decreased (Fig. 7C, red squares). In Fig. 7D, the $t_{1/2}$ was shown to be significantly reduced when comparing before (sweep 5) and after (sweep 20) addition of MTSET. This indicates that MTSET is able to modify the two freely moving VSs in G229C Q-Q* + E1. Addition of 2 mM MTSET to cells expressing G229C Q-Q + E1 did not alter the activation time course or amount of instantaneous current (Fig. 7B). The decrease in peak current seen toward the end of the recording is similar to the rundown observed in WT channels in the absence of MTSET (SI Appendix, Fig. S10H). Furthermore, there was no decrease in the $t_{1/2}$ after addition of MTSET (Fig. 7C, blue triangles), with no

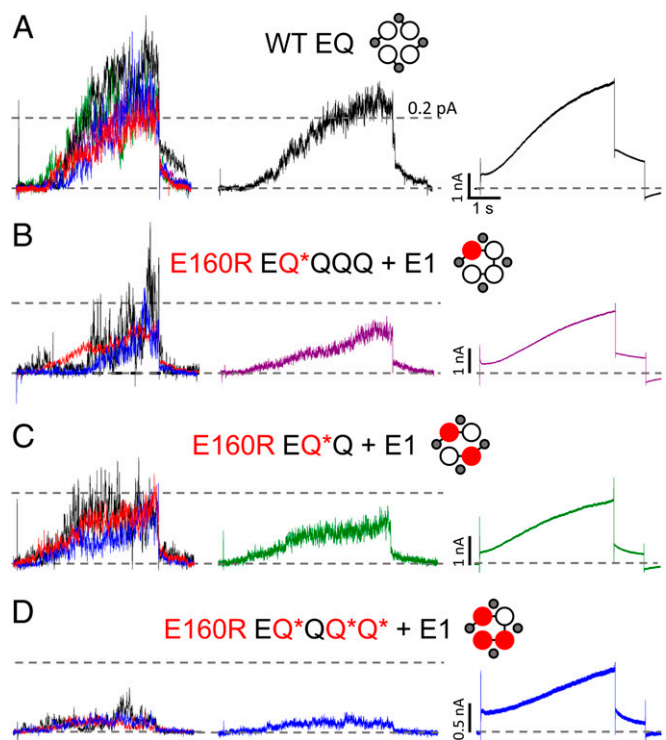


Fig. 6. Ensemble averages of E160R single-channel recordings. Ensemble averages of single-channel data are shown for individual cells (Left), all sweeps together (Middle), and whole-cell recordings (Right) for WT EQ (A), E160R EQ*QQQ + E1 (B), E160R EQ*Q + E1 (C), and E160R EQ*QQ*Q* + E1 (D). WT EQ individual cell ensembles (A, Left) are displayed in green (6 sweeps), black (8 sweeps), red (12 sweeps), blue (10 sweeps), and purple (13 sweeps) (49 sweeps total; $n = 5$). E160R EQ*QQQ + E1 individual cell ensembles (B, Left) are displayed in red (35 sweeps), black (3 sweeps), and blue (11 sweeps) (49 sweeps total; $n = 3$). E160R EQ*Q + E1 individual cell ensembles (C, Left) are displayed in red (24 sweeps), black (10 sweeps), and blue (12 sweeps) (46 sweeps total; $n = 3$). E160R EQ*QQ*Q* + E1 individual cell ensembles (D, Left) are displayed in red (21 sweeps), black (7 sweeps), and blue (29 sweeps) (57 sweeps total; $n = 3$). Individual cell ensembles were refiltered at 200 Hz. Cells were pulsed to $+60$ mV for 4 s, followed by a tail current at -40 mV.

significant change in the $t_{1/2}$ before (sweep 5) or after (sweep 20) addition of 2 mM MTSET (Fig. 7D). This result shows that the E160R mutation in the same subunits as G229C prevents the G229C from being modified by MTSET when channels are activated. This suggests that the presence of the E160R mutation in a VS is able to prevent its outward translation during channel activation, and supports the idea that VSs containing E160R are prevented from reaching an activated conformation.

Voltage-clamp fluorometry (VCF) was used as an alternative method to follow the displacement of VSs during activation. Previously, other groups had shown that the labeling of a cysteine at the top of the S4 of Q1, G219C, with Alexa 488 C₅-maleimide allows tracking of VS environment change during activation of the I_{Ks} channel in oocytes (13, 23). When a channel where G219C is located in all four VSs with a cysteine-less background (G219C Q) was expressed with E1 in oocytes, a current with a $V_{1/2}$ of 20.9 mV resulted (Fig. 8B, Upper, Fig. 8E, and SI Appendix, Table S1). As previously shown (23), fluorescence movement (Fig. 8B, Lower) occurs in two steps, with one step occurring at quite negative potentials and the second step occurring at higher voltages, where pore opening occurs (Fig. 8E).

To confirm that E160R prevents activating VS movements and a change in the fluorophore environment, QQ fusion constructs with a cysteine-less background were used. In the first construct, G219C was in one Q1 and the other Q1 contained the E160R mutation (G219C Q-Q*). A second construct was made where the G219C and E160R mutations were in the same Q1 (G219C Q*-Q). Expression of both of these constructs in oocytes, with E1 (Fig. 8C and D, Upper and Fig. 8E), produced currents with a similar $V_{1/2}$ of activation to G219C Q + E1 (19 to 24 mV;

SI Appendix, Table S1), and were both depolarized from a similar QQ fusion construct without the E160R mutation, with a $V_{1/2}$ of 6.1 mV (G219C Q-Q; SI Appendix, Fig. S11 and Table S1). Fluorescence recordings of G219C Q-Q* + E1 (Fig. 8C, Lower) were smaller than that seen in G219C Q + E1, which is to be expected, as two fewer VSs are being tracked. Still, a similar two-step VS movement was detected, albeit with a shallower slope (Fig. 8E). For G219C Q*-Q + E1, fluorescence changes were not observed, indicating that the presence of the E160R mutation was impeding VS movement (Fig. 8D, Lower).

Discussion

The E160R Mutation in One, Two, or Three Q1 Subunits Prevents VSs from Reaching an Activated State, but Does Not Prevent I_{Ks} Current.

Previously, E160R homotetramers expressed in oocytes had been suggested to produce a channel complex in which the VSs were prevented from activating, and the pore had a close to zero open probability as a result (13). The mutation disrupted charge interactions that normally take place in WT channels, wherein the negative glutamic acid at residue 160 interacts with sequential positive charges in the S4, to allow the VS to move between resting and activated conformations (Fig. 2A) (13).

In the present studies, two methods were used to support the notion that the E160R mutation restrains VSs from moving into their activated conformations. MTSET modification was used to track VS movement directly in mammalian cells (Fig. 7). VSs with a G229C probe in the opposing Q1 subunit from E160R (G229C Q-Q* + E1) were successfully modified by MTSET, demonstrating their freedom to move into the external space. When the E160R mutation and G229C probe were in the same subunit (G229C Q*-Q + E1), modification was no longer observed (Fig. 7B), as would be expected from a restrained VS. The time course of the G229C Q-Q* + E1 currents was very different from those from G229C Q*-Q + E1, with the former activating faster (SI Appendix, Fig. S10A and B). This is likely due to the G229C mutation altering the kinetics of the channel as it activates. As the VSs with the E160R mutation in G229C Q*-Q + E1 are prevented from activating, there was no effect of G229C on the activation of the channel.

VCF experiments confirmed the MTSET results (Fig. 8). Channels with G219C in either the opposite subunit (G219C Q-Q*) or the same subunit (G219C Q*-Q) as E160R were expressed with E1 in oocytes. Voltage-dependent VS fluorescence was detected in G219C Q-Q* + E1 (Fig. 8C) but not in G219C Q*-Q + E1 (Fig. 8D), indicating that the E160R mutation in the same subunit prevented a change in the environment of G219C. Additionally, the G219C mutation increased the rate of deactivation when it was free to move (G219C Q + E1, G219C Q-Q* + E1, and G219C Q-Q + E1; Fig. 8B and C and SI Appendix, Fig. S11A). However, when E160R was in the same subunit, the deactivation kinetics at -40 mV were slower (Fig. 8D), which suggests that G219C was unable to alter channel kinetics due to those VSs being prevented from activating.

To examine ion currents, a range of channel complexes were created where either one, two, three, or four VSs contained the E160R mutation (Q*QQQ, Q*Q, QQQ*Q*, EQ*QQ*Q*, and EQ*, respectively). For channels expressed both in the absence (SI Appendix, Fig. S1) and presence (Figs. 3 and 5) of E1, functional currents were visualized, except in the case of EQ* (Fig. 2). Incorporation of E160R into all four subunits produced a channel that did not pass current. This lack of current was probably not due to a trafficking problem (see above and ref. 32), but may be due to the very low open probability of the channel pore when VSs cannot reach an activated conformation. Whole-cell and single-channel recordings showed that, with each additional E160R mutation in the I_{Ks} channel complex, there was a decrease in conductance, as fewer VSs were able to activate (Figs. 5 and 6 and SI Appendix, Fig. S4). These results suggest that at least one VS is

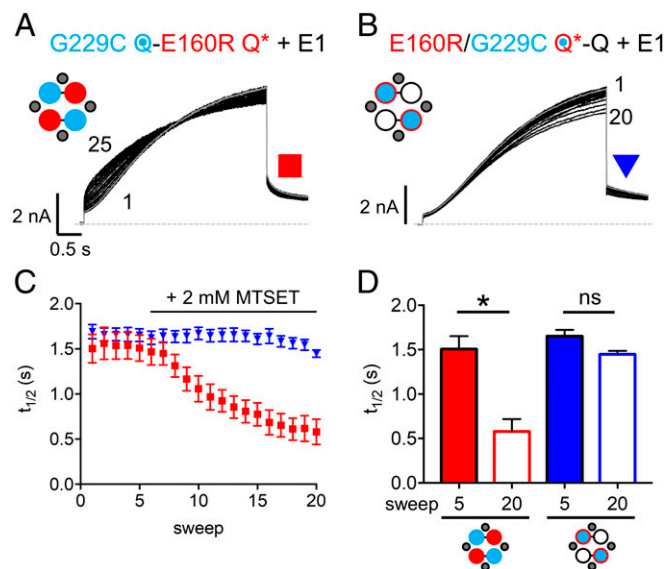


Fig. 7. Extracellular MTSET is unable to modify subunits containing the E160R mutation. Diary plots of currents were obtained via a protocol where cells were held at -90 mV, and pulsed to +60 mV for 4 s and -40 mV for 0.9 s. The sweep-to-sweep interval was 20 s. (A and B) Representative currents are shown for G229C Q-E160R Q* + E1 (A) and E160R/G229C Q*-Q + E1 (B). Sweep 5 is highlighted in gray. After a stable baseline of 5 sweeps, 2 mM MTSET was applied at sweep 6. Cartoons describe the mutations in the constructs: E1 (small gray circles), WT Q1 (unfilled circles), E160R Q1 (red circles), G229C Q1 (blue circles), and E160R/G229C Q1 (blue circles with red border). Black lines indicate tethers between subunits. (C) A diary plot showing time to half-maximum peak current ($t_{1/2}$) plotted versus sweep number for G229C Q-E160R Q* + E1 (red squares) and E160R/G229C Q*-Q + E1 (blue triangles) ($n = 6$ to 8). (D) Plot comparing $t_{1/2}$ for both G229C Q-E160R Q* + E1 and E160R/G229C Q*-Q + E1 before (sweep 5) and after (sweep 20) addition of MTSET (* $P < 0.05$; ns, not significant). Error bars denote mean \pm SE.

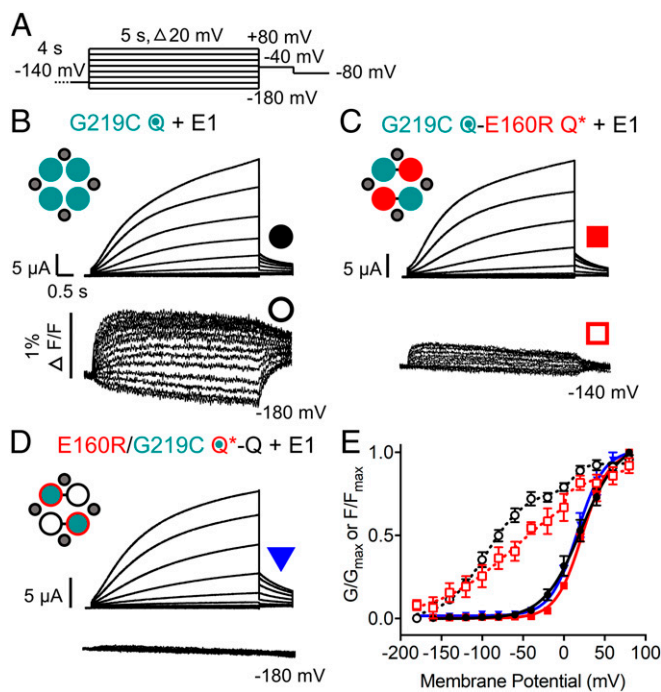


Fig. 8. Fluorescence changes are not detected in subunits containing the E160R mutation. (A) Recordings were obtained using the protocol shown. Sweep-to-sweep intervals were 15 s. (B–D) Representative currents (Upper) and fluorescence recordings (Lower) are shown for G219C Q + E1 (B), G219C Q-E160R Q* + E1 (C), and E160R/G219C Q*-Q + E1 (D). Cartoons describe the mutations in the constructs: E1 (small gray circles), WT Q1 (unfilled circles), E160R Q1 (red circles), G219C Q1 (teal circles), and E160R/G219C Q1 (teal circles with red border). Black lines indicate tethers between subunits. (E) G–V and F–V plots of G219C Q + E1 (G–V: closed black circles; F–V: open black circles), G219C Q-E160R Q* + E1 (G–V: closed red squares; F–V: open red squares), and E160R/G219C Q*-Q + E1 (G–V: closed blue triangles) ($n = 3$ to 8). Error bars denote mean \pm SE.

required to move within the I_{Ks} channel complex to permit detectable ion conduction at the whole-cell level, but that neither Q1 alone, nor the I_{Ks} complex, requires a concerted transition of all four activated VSs to occur in order for the pore to open.

Normal Incorporation of E160R. It was important to establish that E160R subunits incorporated normally when expressed as linked constructs with WT subunits. Using TEA⁺, we have shown that E160R mutated subunits do indeed assemble within the channel complex as expected (*SI Appendix, Fig. S5*), and do not change the sensitivity of V319Y to TEA⁺ (*SI Appendix, Fig. S5D*). Also, altering the order of E160R subunits within the tetramers does not impact the kinetic properties of the expressed constructs (*SI Appendix, Fig. S3*), which again supports the belief that these linked subunits assemble as expected. However, while the data suggest that the ordering of subunits and the presence of the E160R mutation have minimal impact on the average stoichiometry of channels, we acknowledge that the various controls cannot guarantee the stoichiometries depicted for every channel expressed. We also note potential limitations associated with MTSET and VCF recordings. It is possible that the presence of the E160R mutation could prevent G229C modification or G219C labeling by modifying solvent accessibility to these cysteines. Additionally, the E160R mutation might potentially alter the fluorophore environment, so that fluorescence changes upon S4 translation are no longer visible.

Previous Fluorescence and Thermodynamic Studies and Contrasting Models. When Q1 is expressed without E1, the voltage dependence of VS movement measured using Alexa 488 VCF overlaps that of

channel conductance, indicating that movement of individual VSs can lead to channel pore opening (22) and current flow before all VSs have moved, thus obviating the need for a concerted transition of all activated subunits for this to occur. Furthermore, Q1 has a constitutively active current even at very low voltages (25), suggested to reflect transition to an open state independent of any VS movement. Zaydman et al. (31) used a mutation to lock the Q1 pore open, and noted that although the pore remained locked open, the VSs were able to move to a resting conformation. A similar dissociation of the domains is apparent in the Q1 cryo-EM structure, which shows an activated VS but closed pore in the absence of PIP₂ (36). Altogether, these results suggest that Q1 pore opening and VS activation are not rigidly coupled via a concerted gating step(s) but instead are rather loosely coupled during channel activation and deactivation. This is represented by the opening of the pore from multiple VS conformations in the allosteric model in Fig. 1B.

In the presence of E1, however, there are some common experimental findings but different conclusions. Barro-Soria et al. (23) showed, again using fluorescence, that E1 divides VS movement into two steps. The first step of voltage-dependent fluorescence movement in I_{Ks} occurs at more negative potentials than channel conductance, while the second takes place at channel opening potentials. The authors suggested that there are independent VS movements of four Q1 subunits, accounting for the first step, followed by a second concerted conformational step involving all four VSs that allows the pore of the channel to open. This process where four VSs are required to move in a concerted step to allow the pore to conduct is exemplified by an I_{Ks} model set forth by Silva and Rudy (14), and its equivalent is presented in simplified form in Fig. 1A.

Zaydman et al. (13) used charge reversal mutations between the negative E160 in the S2 domain and the positive charges of the S4 domain to suggest that VSs could be in resting, intermediate (E160R/R231E), or fully activated states (E160R/R237E). For Q1 alone, VSs in intermediate states promoted pore opening, represented by the overlap between the G–V and the first component of the F–V curves. In the presence of E1, the pore was prevented from opening at intermediate VS states, but when each VS reached the fully activated state, represented as an overlap between the G–V and the second component of the F–V, E1 potentiated pore opening in an allosteric manner. The suggestion was that the first component of the F–V represented VS movement from a resting to an intermediate state, while the second component perhaps represented movement of the VS to an activated conformation. More recently, Hou et al. (37) demonstrated the presence of two fluorescent components in the activation of VS in Q1 alone, attributed to resting-to-intermediate and intermediate-to-activated conformational changes.

Our experiments with G219C Q-Q* + E1 (Fig. 8) also demonstrated two fluorescence steps in activatable VSs, which were complexed in channels with two nonactivatable VSs. The data suggest that the second fluorescence step may not require the concerted rearrangement of all four VSs but that at least one VS has to be activatable, in support of the conclusions of Zaydman et al. (13) and Hou et al. (37). It should be noted that other contributions to a secondary fluorescence movement potentially include a secondary rearrangement of the channel complex at higher membrane potentials or displacement of E1, which alters the fluorophore environment and the fluorescence emission signal. As such, it seems that additional experiments are required to fully understand this two-step fluorescence signal.

Meisel et al. (24) used thermodynamic mutant cycle analysis to investigate the effect on channel gating of a loss-of-function mutation located at the bottom of the S4 domain, R243W. If this mutation was incorporated into one, two, three, or all four Q1 subunits, there was a progressive displacement of channel opening to more depolarized potentials in the presence of E1.

The authors concluded that the linear correlation between the depolarizing shift of the $V_{1/2}$ and the number of mutated subunits indicated independent and sequential VS movement, and that channel opening did not require a concerted activation step.

Loose Coupling Between VS Activation and Pore Opening: Effects on Whole-Cell and Single-Channel Kinetics. The data presented here show that up to three VSs can be prevented from activating, while the channel may still open and produce currents with sigmoidal activation and voltage-dependent kinetics. The depolarizing shifts in the isochronal activation $V_{1/2}$ s seem relatively mild, with little change when one VS contains E160R, and a depolarization of only ~30 mV when three of four subunits contain the E160R mutation (Fig. 3 and *SI Appendix, Table S1*). As noted by Meisel et al. (24), who measured very low intersubunit coupling free energies for multiple R243W mutations, these results suggest very loose VS coupling to overall closed and open channel conformations.

Unlike the data from R243W, with either E160R or F57W there was no simple relationship between the number of mutant VSs and the change in $V_{1/2}$ (Fig. 3 and *SI Appendix, Fig. S9*). With one E160R VS (Q*QQQ) in the presence or absence of E1, there was no statistically significant shift in the $V_{1/2}$ of activation (Fig. 3 and *SI Appendix, Fig. S1*). With two E160R VSs (Q*Q) in the presence or absence of E1, there was a depolarizing shift of ~16 mV, and a further 12-mV change between two and three E160R VSs (Q*Q + E1 vs. EQ*QQ*Q* + E1) (Fig. 3). Similarly, for F57W in E1, which is known to shift the I_{Ks} $V_{1/2}$ of activation to greater than 100 mV when present in all four copies in the octameric complex (30). Compared with control, when one, two, or four F57W mutations are present in the I_{Ks} channel complex, the G–V curve $V_{1/2}$ s were unchanged (34.8 mV), or depolarized by ~8 mV (42.3 mV) or to 106 mV, respectively (*SI Appendix, Fig. S9 A–D and Table S1*), albeit accompanied by a large decrease in the overall voltage sensitivity.

Loose coupling of pore opening to individual VS activation (Fig. 1B) may also explain multiple subconductance states observed in WT I_{Ks} single-channel recordings (10, 34, 38), and in the present experiments with different numbers of mutant E160R VSs present (Fig. 5). As more VSs contain the E160R mutation, currents are still visible, but conductance is progressively reduced as a result of the lower open-state stability and/or increased closed-state stability, seen as increased flickering in single-channel openings (Fig. 5). Long interburst closings are observed, as well as small subconductance events that never lead to larger openings (*SI Appendix, Fig. S9E*, e.g., *Left*, second sweep). Similar results were seen from F57W (*SI Appendix, Fig. S9*), although there are subtle differences at the single-channel level. As the F57W mutation does not prevent activation of the VS via electrostatic repulsion like E160R, the channel may be more likely to continue to burst open once the pore begins to conduct, and visit higher conducting states.

In Kv2.1 (39), partially activated channels are also able to visit subconducting states, so that movement of a single VS to an activated conformation is sufficient for the channel to conduct current, with each additional VS movement increasing conductance. Furthermore, it was noted that when VSs are all in the same “homomeric” position (four resting or four activated), they were in their most stable conformation (39), whereas when only one VS activated, a “heteromeric” conformation was achieved that resulted in much less stable current sublevels (39, 40), implying that there are stabilizing interactions that occur between the four subunits (39).

A Model Coupling Activation of Individual VSs to the Pore Opening.

We used a model of allosteric gating for I_{Ks} like that shown in Fig. 1B to understand the implications of the experimental observations of this study. These include: nonlinear changes in the $V_{1/2}$ of activation (Fig. 3 and *SI Appendix, Figs. S1 and S9D*); small changes in activation delays and overall activation time course (Fig. 4A); speeding of tail currents seen with increasing

numbers of E160R VSs (Fig. 4B); and the decreased conductance seen with increasing numbers of E160R VSs (Fig. 5 and *SI Appendix, Fig. S4*). E160R data were simulated using a recent model of I_{Ks} gating, published by Zaydman et al. (13), which assumes independent VS movement, including two transitions during VS activation and a detailed description of VS domain-pore coupling. The scheme for voltage-dependent gating is shown in Fig. 9A, and expanded schemes and rates used in the individual models for VSs containing one, two, or three E160R subunits may be found in *SI Appendix, Materials and Methods and Fig. S12*. A key feature of the Zaydman model is VS–pore coupling constants (θ_{RC} , etc.) specific for resting, intermediate, and activated VS states (Fig. 9A and *SI Appendix, Tables S2–S4*).

The original published model was optimized for data obtained from *Xenopus* oocytes, and it was necessary to alter voltage-dependent rate constants between VS states as well as the intrinsic C→O and O→C rates to better match the kinetics of our data from mammalian cells. The updated voltage dependencies of rate constants for the VS R→I and I→A transitions are shown in *SI Appendix, Fig. S13*, and all of the rates and constants are listed in *SI Appendix, Tables S2–S4*.

The E160R mutation turns the VS into a domain that no longer contributes to channel activation and cannot reach intermediate closed states, as Q1 subunits expressed alone do not show measurable current (13, 29, 32) and therefore VSs must not reach intermediate closed states. This was represented by modifying the model to include only three, two, or one VS domains in Q*QQQ, Q*Q, and Q*QQ*Q*, respectively (*SI Appendix, Fig. S12*). The predicted currents and current-voltage relationships are shown in Fig. 9B and C, and G–V relationships are shown in Fig. 9D. The simulated currents all show delayed and sigmoidal activation, similar to the experimental results, with a reduced whole-cell current density as the number of E160R VSs is increased (Fig. 9B and C). The current reduction is quite similar to that seen experimentally (*SI Appendix, Fig. S4*), with a 60% reduction in the current density of the two-E160R VS model (equivalent to Q*Q + E1) and an 81% reduction in the model with three E160R VSs. However, it should be noted that model data cannot account for expression issues that may occur with experimental constructs and contribute to changes in expressed current density.

The $V_{1/2}$ s of the simulated G–V relationships were depolarized by 0, 3, and 18 mV for one, two, or three E160R subunits, respectively (Fig. 9D), which is nonlinear but proportionally less than seen with the experimental data (*SI Appendix, Table S1*). The slopes of the G–V relationships in the model, with the exception of the three-E160R VS model, are very similar to those observed experimentally at 21.6, 21.0, and 23.1 mV for WT and one- and two-E160R VSs, respectively. The slope for the G–V of the three-E160R VS model was 33.4 mV, much shallower than the experimental value (22.7 mV; *SI Appendix, Table S1*), and this may be a result of fewer VS transition steps in the model than in real channel complexes. But, interestingly, that value is quite similar to the G–V slope for F57W E/Q (33.8 mV) and, as well, the slope of E160R Q*Q in the absence of E1 is shallower than the control (*SI Appendix, Fig. S1*). The model simulations of tail currents depicted in Fig. 9E, *Upper* were accelerated in a similar manner to that seen experimentally with increased numbers of E160R VSs (Fig. 9E, *Lower*).

Overall, the allosteric model reproduces the experimental findings well, including the nonlinear displacement of the $V_{1/2}$ to more positive potentials, the speeding of tail currents with additional E160R subunits, and the decreasing voltage sensitivity of the G–V relationship. The quantitative underestimation of the magnitudes of the depolarizing shifts in the $V_{1/2}$ to more positive potentials may reflect the difficulty in obtaining saturating activation relationships in the experiments due to the very slow activation of I_{Ks} currents, or not quite ideal selection of rate constants in the models. Further studies and model development are required to fully understand these differences.

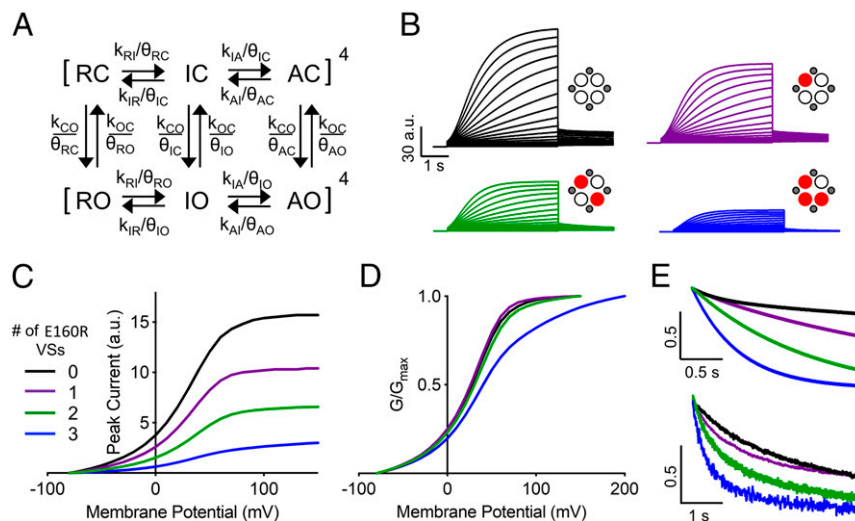


Fig. 9. Simulations produced by an allosteric model with E160R mutant VSs reproduce experimental results. (A) Modified from ref. 13, which is licensed under CC BY 4.0. Resting, intermediate, and activated closed states are represented by RC, IC, and AC, respectively. Resting, intermediate, and activated open states are represented by RO, IO, and AO, respectively. Voltage-dependent transition rates of the VS are denoted by k_{RI} , k_{IR} , k_{IA} , and k_{AI} . Transitions rates between open and closed states are denoted by k_{CO} and k_{OC} . VS–pore interactions are represented by θ parameters. Rates and constants are as described in *SI Appendix, Materials and Methods and Tables S2–S4*. (B) Simulated I_{K_S} currents between -80 and $+100$ mV are shown for channels with no (black traces), one (purple traces), two (green traces), and three (blue traces) E160R VSs. The protocol was set from -80 to $+100$ mV for 4 s, with a 2-s tail current at -50 mV. The scale is in arbitrary units (a.u.). (C and D) Current–voltage (C) and conductance–voltage (D) plots are shown for simulated data where no (black line), one (purple line), two (green line), and three (blue line) VSs contain E160R. In C, the scale is in arbitrary units. (E) Tail currents normalized to the peak current at -50 mV after a 4-s pulse to $+60$ mV of simulated (Upper) and experimental data (Lower) are shown for no (black), one (purple), two (green), and three (blue) E160R VSs.

Functional Implications of Allosteric Coupling Between VS Activation and Pore Opening in I_{K_S}

Allosteric gating of I_{K_S} potentially allows for a channel that can be highly regulated at different stages in the activation process by a variety of different factors. This is exemplified by the actions of a cAMP analog on I_{K_S} , which can be localized to the VS and causes a hyperpolarization of the $V_{1/2}$, increasing open probability and current density (41, 42). I_{K_S} combines flexible stoichiometry, where up to four E1 subunits can complex with the Q1 channel tetramer (9, 10), with loose coupling between VSs and pore opening and the lack of a requirement for a concerted step during opening. This suggests that the effect that E1 has on a single VS during activation (23) will not constrain the behavior of the other VSs but that all of them together will determine the subsequent nature of pore kinetics. This possibility is of further interest, as Q1 can be regulated by a variety of accessory subunits (KCNE1 to 5) (1), which all have different actions on the VSs. For example, in contrast to E1, KCNE3 promotes VS activation and produces channels with a very high open probability at more hyperpolarized potentials (43). As several of the accessory subunits have been colocalized within the same tissues (44), it is possible that there could be a mixed population of KCNE subunits interacting with the same Q1 tetramer, with each KCNE exerting its own effects on individual VSs, and through them to the pore.

Conclusions

By studying the electrophysiology of I_{K_S} complexes where one, two, three, or four VSs were prevented from reaching their activated conformations, we have shown that not all four VSs are required to move and act in a concerted manner to allow the Q1 pore to conduct current in the presence and absence of E1. Instead, Q1 and I_{K_S} channel complexes gate allosterically, while individual and loosely coupled VS movements allow for highly flexible and regulated opening of the pore.

Materials and Methods

See *SI Appendix* for the materials and methods for chemicals, molecular biology, cell culture and transfection, oocyte preparation, whole-cell, single-channel, and VCF electrophysiology solutions, data analysis, and modeling. Oocytes were prepared in accordance with the University of British Columbia Animal Care Protocol (Certificate #A18-0074).

ACKNOWLEDGMENTS. We thank Dr. Jianmin Cui for the C214A/G219C/C331A Q1 construct, and Dr. Yoshihiro Kubo for the pGEMHE vector. We thank Dr. Logan Macdonald, Dr. Ying Dou, and Fariba Ataei for their technical assistance. This research was supported by the Natural Sciences and Engineering Research Council of Canada (Grant RGPIN-2016-05422), Canadian Institutes of Health Research (Grant PJT-156181), and Heart and Stroke Foundation of Canada (Grant G17-0018392) (to D.F.). M.W. held a graduate research scholarship from the University of British Columbia.

- Liin SI, Barro-Soria R, Larsson HP (2015) The KCNQ1 channel—Remarkable flexibility in gating allows for functional versatility. *J Physiol* 593:2605–2615.
- Belloccq C, et al. (2004) Mutation in the KCNQ1 gene leading to the short QT-interval syndrome. *Circulation* 109:2394–2397.
- Franqueza L, et al. (1999) Long QT syndrome-associated mutations in the S4-S5 linker of KvLQT1 potassium channels modify gating and interaction with minK subunits. *J Biol Chem* 274:21063–21070.
- Splawski I, et al. (2000) Spectrum of mutations in long-QT syndrome genes. KVLQT1, HERG, SCN5A, KCNE1, and KCNE2. *Circulation* 102:1178–1185.
- Plant LD, Xiong D, Dai H, Goldstein SAN (2014) Individual IKs channels at the surface of mammalian cells contain two KCNE1 accessory subunits. *Proc Natl Acad Sci USA* 111:E1438–E1446.
- Wang KW, Goldstein SA (1995) Subunit composition of minK potassium channels. *Neuron* 14:1303–1309.
- Morin TJ, Kobertz WR (2008) Counting membrane-embedded KCNE beta-subunits in functioning K^+ channel complexes. *Proc Natl Acad Sci USA* 105:1478–1482.
- Chen H, Kim LA, Rajan S, Xu S, Goldstein SA (2003) Charybdotoxin binding in the I(Ks) pore demonstrates two MinK subunits in each channel complex. *Neuron* 40:15–23.
- Nakajo K, Ulbrich MH, Kubo Y, Isacoff EY (2010) Stoichiometry of the KCNQ1–KCNE1 ion channel complex. *Proc Natl Acad Sci USA* 107:18862–18867.
- Murray CI, et al. (2016) Unnatural amino acid photo-crosslinking of the IKs channel complex demonstrates a KCNE1:KCNQ1 stoichiometry of up to 4:4. *eLife* 5:e11815.
- Wang K, et al. (2011) Biophysical properties of slow potassium channels in human embryonic stem cell derived cardiomyocytes implicate subunit stoichiometry. *J Physiol* 589:6093–6104.
- Wang W, Xia J, Kass RS (1998) MinK-KvLQT1 fusion proteins, evidence for multiple stoichiometries of the assembled IsK channel. *J Biol Chem* 273:34069–34074.

13. Zaydman MA, et al. (2014) Domain-domain interactions determine the gating, permeation, pharmacology, and subunit modulation of the IKs ion channel. *eLife* 3: e03606.
14. Silva J, Rudy Y (2005) Subunit interaction determines IKs participation in cardiac repolarization and repolarization reserve. *Circulation* 112:1384–1391.
15. Hodgkin AL, Huxley AF (1952) A quantitative description of membrane current and its application to conduction and excitation in nerve. *J Physiol* 117:500–544.
16. Zagotta WN, Hoshi T, Aldrich RW (1994) Shaker potassium channel gating. III: Evaluation of kinetic models for activation. *J Gen Physiol* 103:321–362.
17. Schoppa NE, Sigworth FJ (1998) Activation of Shaker potassium channels. III. An activation gating model for wild-type and V2 mutant channels. *J Gen Physiol* 111: 313–342.
18. Bezanilla F, Perozo E, Stefani E (1994) Gating of Shaker K⁺ channels: II. The components of gating currents and a model of channel activation. *Biophys J* 66:1011–1021.
19. Mannuzzo LM, Isacoff EY (2000) Independence and cooperativity in rearrangements of a potassium channel voltage sensor revealed by single subunit fluorescence. *J Gen Physiol* 115:257–268.
20. Pathak M, Kurtz L, Tombola F, Isacoff E (2005) The cooperative voltage sensor motion that gates a potassium channel. *J Gen Physiol* 125:57–69.
21. Cha A, Bezanilla F (1997) Characterizing voltage-dependent conformational changes in the Shaker K⁺ channel with fluorescence. *Neuron* 19:1127–1140.
22. Osteen JD, et al. (2010) KCNE1 alters the voltage sensor movements necessary to open the KCNQ1 channel gate. *Proc Natl Acad Sci USA* 107:22710–22715.
23. Barro-Soria R, et al. (2014) KCNE1 divides the voltage sensor movement in KCNQ1/KCNE1 channels into two steps. *Nat Commun* 5:3750.
24. Meisel E, et al. (2012) KCNQ1 channels do not undergo concerted but sequential gating transitions in both the absence and the presence of KCNE1 protein. *J Biol Chem* 287:34212–34224.
25. Ma LJ, Ohmert I, Vardanyan V (2011) Allosteric features of KCNQ1 gating revealed by alanine scanning mutagenesis. *Biophys J* 100:885–894.
26. Horrigan FT, Cui J, Aldrich RW (1999) Allosteric voltage gating of potassium channels I. Msls ionic currents in the absence of Ca(2+). *J Gen Physiol* 114:277–304.
27. Cui J (2016) Voltage-dependent gating: Novel insights from KCNQ1 channels. *Biophys J* 110:14–25.
28. Ramasubramanian S, Rudy Y (2018) The structural basis of IKs ion-channel activation: Mechanistic insights from molecular simulations. *Biophys J* 114:2584–2594.
29. Restier L, Cheng L, Sanguinetti MC (2008) Mechanisms by which atrial fibrillation-associated mutations in the S1 domain of KCNQ1 slow deactivation of IKs channels. *J Physiol* 586:4179–4191.
30. Chen H, Goldstein SAN (2007) Serial perturbation of MinK in IKs implies an alpha-helical transmembrane span traversing the channel corpus. *Biophys J* 93:2332–2340.
31. Zaydman MA, et al. (2013) Kv7.1 ion channels require a lipid to couple voltage sensing to pore opening. *Proc Natl Acad Sci USA* 110:13180–13185.
32. Wu D, et al. (2010) State-dependent electrostatic interactions of S4 arginines with E1 in S2 during Kv7.1 activation. *J Gen Physiol* 135:595–606.
33. Kurokawa J, Motoike HK, Kass RS (2001) TEA(+)-sensitive KCNQ1 constructs reveal pore-independent access to KCNE1 in assembled I(Ks) channels. *J Gen Physiol* 117: 43–52.
34. Werry D, Eldstrom J, Wang Z, Fedida D (2013) Single-channel basis for the slow activation of the repolarizing cardiac potassium current, I(Ks). *Proc Natl Acad Sci USA* 110:E996–E1005.
35. Rocheleau JM, Kobertz WR (2008) KCNE peptides differently affect voltage sensor equilibrium and equilibration rates in KCNQ1 K⁺ channels. *J Gen Physiol* 131:59–68.
36. Sun J, MacKinnon R (2017) Cryo-EM structure of a KCNQ1/CaM complex reveals insights into congenital long QT syndrome. *Cell* 169:1042–1050.e9.
37. Hou P, et al. (2017) Inactivation of KCNQ1 potassium channels reveals dynamic coupling between voltage sensing and pore opening. *Nat Commun* 8:1730.
38. Yang Y, Sigworth FJ (1998) Single-channel properties of IKs potassium channels. *J Gen Physiol* 112:665–678.
39. Chapman ML, VanDongen HM, VanDongen AM (1997) Activation-dependent subconductance levels in the drk1 K channel suggest a subunit basis for ion permeation and gating. *Biophys J* 72:708–719.
40. Chapman ML, VanDongen AM (2005) K channel subconductance levels result from heteromeric pore conformations. *J Gen Physiol* 126:87–103.
41. Thompson E, et al. (2017) cAMP-dependent regulation of I_{Ks} single-channel kinetics. *J Gen Physiol* 149:781–798.
42. Terrenoire C, Clancy CE, Cormier JW, Sampson KJ, Kass RS (2005) Autonomic control of cardiac action potentials: Role of potassium channel kinetics in response to sympathetic stimulation. *Circ Res* 96:e25–e34.
43. Barro-Soria R, Perez ME, Larsson HP (2015) KCNE3 acts by promoting voltage sensor activation in KCNQ1. *Proc Natl Acad Sci USA* 112:E7286–E7292.
44. Bendahhou S, et al. (2005) In vitro molecular interactions and distribution of KCNE family with KCNQ1 in the human heart. *Cardiovasc Res* 67:529–538.